UCRL-JC-105569
PREPRINT

Phase Stability of a Standing-Wave Free-Electron Laser

W. M. Sharp
Lawrence Livermore National Laboratory, University of California
Livermore, California 94550

G. Rangarajan and A. M. Sessler
Lawrence Berkeley Laboratory, Berkeley, California 94720

J. S. Wurtele
Massachusetts Institute of Technology
Cambridge, MA 02139

This paper was prepared for submittal to the
Intense Microwave and Particle Beams, II, OE/LASE '91
January 20-25, 1991, Los Angeles, CA

January 1991

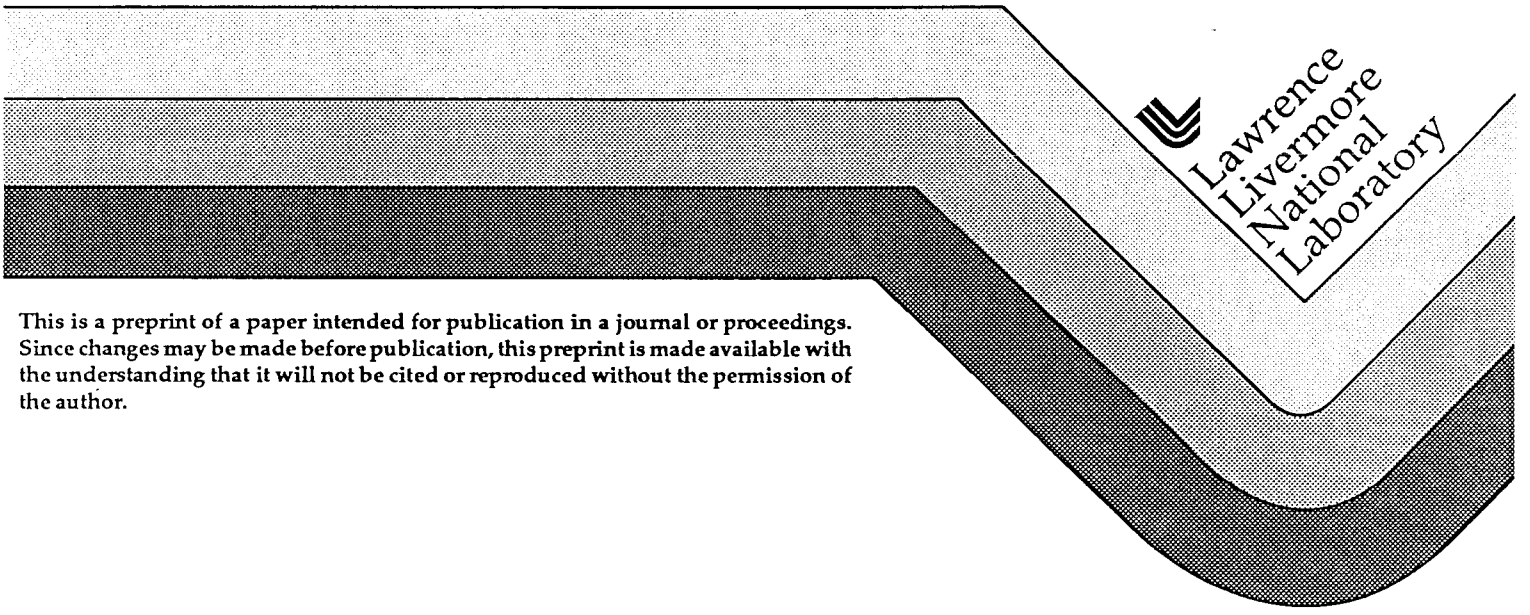

Phase stability of a standing-wave free-electron laser

W. M. Sharp
Lawrence Livermore National Laboratory, University of California
Livermore, California 94550

G. Rangarajan and A. M. Sessler
Lawrence Berkeley Laboratory
Berkeley, CA 94720

J. S. Wurtele
Massachusetts Institute of Technology
Cambridge, MA 02139

ABSTRACT

The standing-wave free-electron laser (FEL) differs from a conventional linear-wiggler microwave FEL in using irises along the wiggler to form a series of standing-wave cavities and in reaccelerating the beam between cavities to maintain the average energy. The device has been proposed for use in a two-beam accelerator because microwave power can be extracted more effectively than from a traveling-wave FEL. A simplified numerical simulation indicates that, with appropriate prebunching, the standing-wave FEL can produce an output signal that is effectively the same in all cavities. However, changes in the beam energy of less than 1% are found to introduce unacceptably large fluctuations of signal phase along the device. Analytic calculations and single-particle simulations are used here to show that the phase fluctuations result from beam synchrotron motion in the initial signal field, and an approximate analytic expression for the signal phase is derived. Numerical simulations are used to illustrate the dependence of phase fluctuations on the beam prebunching, the beam-current axial profile, and the initial signal amplitude.

1. INTRODUCTION

Conceptual designs for a two-beam accelerator (TBA) using a free-electron laser (FEL) as the microwave source[1] have faced two principal problems. Experiments[2] have shown that the large signal amplitude in such devices leads to electrical breakdown near septa used to extract the power, and breakdown is also considered likely in the reacceleration cells used to maintain the beam energy. In addition, theoretical work predicts that small errors in the drive-beam energy introduce a frequency shift that causes a cumulative phase change along the wiggler.

The coupled-cavity TBA[3,4] was devised to avoid the breakdown problem. In this device, irises are placed along the FEL wiggler to form a series of microwave cavities, and induction cells are placed between cavities to reaccelerate the beam. The standing-wave signal that builds up in the cavities as the beam passes through is coupled to a parallel high-gradient radio-frequency (RF) accelerator. This coupling scheme was proposed by Henke[5] and is analyzed elsewhere[4]. Previous one-dimensional simulations[3] of the standing-wave FEL (SWFEL) used in the coupled-cavity TBA indicated that a drive beam which is pre-bunched at a frequency slightly higher than that of the FEL could, with appropriate reacceleration, generate effectively the same final signal amplitude in all cavities. The device was also shown to be weakly affected by errors in the beam current and in the amplitude and timing of the reacceleration field. However, errors in beam energy of less than 1% were found to cause long-wavelength fluctuations in the signal phase of up to two radians. Although this phase ripple is an improvement over the secular phase change found with a conventional FEL, it nonetheless decreases the average microwave field in the high-gradient structure and consequently introduces an unacceptable error in the momentum of the high-energy beam.

In this paper, we model the standing-wave FEL by a set of linearized single-particle equations and examine the phase-stability problem using analysis and numerical solution of the equations. The model is discussed briefly in Section 2, and in Section 3, we summarize approximate solutions of the equations by a finite-series technique

and by separation of variables. These analytic results are corroborated and generalized by numerical simulations presented in Section 4. In a concluding section, we summarize the principal results and discuss what constraints the signal-phase fluctuations impose on drive-beam energy stability.

2. MODEL

2.1 Assumptions and equations

As in previous SWFEL simulations[3], the beam emittance is assumed small enough that radial motion and the effects of the transverse beam structure may be neglected. This one-dimensional beam is taken to couple only with a TE_{01} waveguide mode, which is usually most strongly driven mode. The signal wavenumber for this mode in a rectangular waveguide with height h and width w is $k_s = (\omega_s^2/c^2 - \pi^2/h^2)^{1/2}$. For the fields, we assume an idealized linear wiggler with a vector potential

$$\underset{\sim}{A}_w = \frac{m_e c^2}{e} a_w \cos(k_w z)\ \hat{\mathbf{x}} \tag{1}$$

and an appropriate form for the signal field

$$\underset{\sim}{A}_s = -\frac{m_e c^2}{e} a_s\ \underset{\sim}{q}_\perp (x,y) \cos(k_s z - \omega_s t + \phi), \tag{2}$$

where $\underset{\sim}{q}_\perp = -\sin(\pi y/h)\ \hat{\mathbf{x}}$ is the transverse structure for a TE_{01} mode. Since resonance in this device is maintained by reaccelerating the beam rather than by adjusting the wiggler strength or wavelength, both a_w and k_w are treated here as constants. A number of other conventional assumptions are made that are suitable for most Compton-regime FELs and significantly simplify the equations. The total energy $\gamma m_e c^2$ of all beam electrons is taken to be sufficiently high that $a_w/\gamma \ll 1$, and the energy spread is assumed small enough that all particles have effectively the same axial velocity V_b. We treat the signal amplitude a_s as small compared with a_w, and the both a_s and ϕ are assumed to be slowly varying compared with $k_s z$ and $\omega_w t$. This last assumption makes the equations inappropriate for modeling waveguide modes near cutoff.

The motion of the jth drive-beam electron is modeled by wiggle-averaged equations for γ_j and the particle phase $\theta_j = (k_s + k_w)z - \omega_s t$ that are identical to those in a conventional single-mode microwave FEL. Taking z to be the independent variable, we write the equations as

$$\frac{d\theta_j}{dz} = k_w + k_s - \frac{\omega_s}{c} - \frac{\omega_s}{2c\gamma_j^2}\left[1 + \frac{a_w^2}{2} - 2D_x a_w\,(\hat{a}_r \cos\theta_j - \hat{a}_i \sin\theta_j)\right] \tag{3a}$$

$$\frac{d\gamma_j}{dz} = -D_x \frac{\omega_s}{c}\frac{a_w}{\gamma_j}\,(\hat{a}_r \sin\theta_j + \hat{a}_i \cos\theta_j) - \frac{eE_z}{m_e c^2}, \tag{3b}$$

where E_z is the external reacceleration field, and $\hat{a}_r$ and $\hat{a}_i$ are components of the complex signal amplitude $\hat{a} \equiv \hat{a}_r + i\hat{a}_i = a_s \exp(i\phi)$. In Eq. (3), the coupling coefficient D_x is given for a TE_{01} mode by

$$D_x = \frac{1}{2}\left[J_0(\xi) - J_1(\xi)\right], \tag{4}$$

where $\xi = \omega_s a_w^2/(8ck_w\gamma_j^2) \approx a_w^2/4(1 + a_w^2/2)$.

An equation for $\hat{a}$ is obtained by assuming that the signal evolves only in time and requiring that the wiggle-averaged equations conserve energy. Taking the distance back from the beam head $s \equiv V_b t - z$ as the "time" coordinate, this procedure gives the field equation

$$\frac{\partial \hat{a}}{\partial s} = i\eta\left\langle \frac{\exp(-i\theta_j)}{\gamma_j} \right\rangle, \tag{5}$$

where the coefficient η in general depends on s and is given by

$$\eta = \frac{4\pi}{hw}\frac{eI_b}{m_e c^3}\frac{c}{V_b}\frac{c}{\omega_s}D_x a_w, \tag{6}$$

where I_b is the beam-current magnitude. This coefficient is exactly half of that found for a traveling-wave FEL because here the current interacts only with the forward-propagating component of the standing-wave signal. While Eq. (5) implicitly assumes an infinitesimal cavity length and ignores field coupling through the cavity irises, it does model the novel signal evolution expected in a SWFEL.

2.2 Linearized equations

The SWFEL equations are reduced to a form suitable for analysis by making a number of simplifying assumptions. We first make the assumption of a "single-particle" distribution, in which the full beam current is assigned to a single phase-space point. The further assumption that the γ remains near the resonant energy

$$\gamma_r^2 = \frac{\omega_s}{2c}\frac{1+\frac{1}{2}a_w^2}{k_w + k_s - \frac{\omega_s}{c}} \tag{7}$$

allows us to linearize the equations in $\Delta\gamma = \gamma - \gamma_r$, leading to the approximate particle equations

$$\frac{d\theta}{dz} \approx 2\left(k_w + k_s - \frac{\omega_s}{c}\right)\frac{\Delta\gamma}{\gamma_r} \tag{8a}$$

$$\frac{d\Delta\gamma}{dz} \approx -D_x\frac{\omega_s}{c}\frac{a_w}{\gamma_r}\left(\hat{a}_r\sin\theta + \hat{a}_i\cos\theta\right) - \frac{eE_z}{m_e c^2}. \tag{8b}$$

If we take the beam current to be constant for $0 \le s \le L_b$, then we obtain a particularly simple linearized equation for $\hat{a}$

$$\frac{\partial\hat{a}}{\partial s} = i\frac{\eta_0}{\gamma_r}\exp(-i\theta), \tag{9}$$

where η_0 is the constant value of η.

A z-independent solution to Eq. (8) is found by first noting that $\Delta\gamma$ is constant when E_z is given by

$$\frac{eE_z}{m_e c^2} \approx -D_x\frac{\omega_s}{c}\frac{a_w}{\gamma_r}\left(\hat{a}_r\sin\theta + \hat{a}_i\cos\theta\right). \tag{10}$$

If $\Delta\gamma$ is initially zero, then θ is likewise independent of z and equal to some arbitrary $\theta_0(s)$. The components of $\hat{a}$ in Eq. (10) are obtained by integrating the linearized field equation, which gives

$$\hat{a}(s) = \hat{a}(0) + \frac{i\eta_0}{\gamma_r}\int_0^s ds'\,\exp[-i\theta_0(s')]. \tag{11}$$

As a practical special case, we consider a constant-current beam that is prebunched at a frequency $\omega_s + \Delta\omega$, so that $\theta_0(s) = \alpha - (\Delta\omega/V_b)s \equiv \alpha + \beta s$. The components of the equilibrium signal field $\hat{a}_0$ are then given by

$$\hat{a}_{0r}(s) = \hat{a}_r(0) + \frac{\eta_0}{\beta\gamma_r}\left[\cos(\alpha) - \cos(\alpha+\beta s)\right] \tag{12a}$$

$$\hat{a}_{0i}(s) = \hat{a}_i(0) - \frac{\eta_0}{\beta\gamma_r}\left[\sin(\alpha) - \sin(\alpha+\beta s)\right], \tag{12b}$$

and the corresponding reacceleration field is

$$\begin{aligned}\frac{eE_z}{m_e c^2} = -D_x\frac{\omega_s}{c}\frac{a_w}{\gamma_r}\Big[&\hat{a}_r(0)\sin(\alpha+\beta s)\\ &+ \hat{a}_i(0)\cos(\alpha+\beta s) + \frac{\eta_0}{\beta\gamma_r}\sin(\beta s)\Big].\end{aligned} \tag{13}$$

We obtain beam and equations for small s-dependent perturbations of this equilibrium by substituting the representations

$$\hat{a}(z,s) = \hat{a}_0(s) + \hat{a}_1(z,s) \tag{14a}$$

$$\theta(z,s) = \theta_0(s) + \theta_1(z,s) \tag{14b}$$

into Eqs. (8) and (11). Eliminating $\hat{a}_1$ and $\Delta\gamma$, we find

$$\frac{d^2\theta_1}{dz^2} + \Omega^2(s)\theta_1 = -\frac{K^2\eta_0}{\gamma_r}\int_0^s ds'\ \theta_1(s')\sin[\beta(s-s')], \tag{15}$$

where the particle synchrotron wavenumber in the unperturbed field is

$$\Omega^2(s) = K^2[\hat{a}_{0r}(s)\cos\theta_0(s) - \hat{a}_{0i}(s)\sin\theta_0(s)], \tag{16}$$

and K^2 is defined by

$$K^2 = 2D_x\left(k_w + k_s - \frac{\omega_s}{c}\right)\frac{\omega_s}{c}\frac{a_w}{\gamma_r^2}. \tag{17}$$

Since we are interested in the effects of small initial beam-energy displacements $\Delta\gamma_0$ from γ_r, appropriate initial conditions for Eq. (15) are

$$\theta_1(0,s) = 0 \tag{18a}$$

$$\frac{d\theta_1}{dz}(0,s) = \frac{\omega_s}{c\gamma_r^3}\left(1 + \frac{1}{2}a_w^2\right)\Delta\gamma_0. \tag{18b}$$

The θ_1 equation has the same form as the equation for transverse displacement due to the beam break-up instability[6], except that the characteristic wavenumber Ω depends on s in this case. In fact, the analogy is quite accurate, since the standing wave left by the beam head acts like a "wake field" that affects electrons in the beam tail. The amplitude and phase perturbations of the FEL signal may be obtained by substituting θ_1 from Eq. (15) into the $\hat{a}_1$ equation

$$\hat{a}_1 = \frac{\eta_0}{\gamma_r}\int_0^s ds'\ \theta_1(s')\exp[-\theta_0(s')]. \tag{19}$$

We note that taking η to be independent of s is not necessary for the analysis here, but the choice simplifies the results without qualitatively altering the behavior of the signal phase.

3. ANALYTIC RESULTS

3.1 Solution by finite-series

The s-dependence of Ω in Eq. (16) makes it impractical to use Laplace-transform techniques to solve Eq. (15) for θ_1. However, if the integral over s is replaced by a finite sum over beam segments of length Δs, with θ_1 and Ω assumed constant within a segment, then the θ_1 equation for each segment is easily Laplace transformed and can be solved in a closed form involving Ω values in that segment and preceding ones. Since the beam is bunched axially in the ponderomotive buckets, this discrete model is, in fact, more realistic than the continuum model, provided that Δs is set to the bucket length $2\pi/(k_s + k_w) \approx 2\pi/k_s$.

From Eq. (15), the discretized equation for θ_1 in the Mth segment may be written

$$\frac{d^2\theta_1}{dz^2}(z,M) + \Omega^2(M\Delta s)\theta_1(z,M) = -\frac{K^2\eta_0\Delta s}{\gamma_r}\sum_{m=0}^{M}\theta_1(z,m)\sin[\beta(M-m)\Delta s]. \tag{20}$$

Since Ω for each segment is constant, the Laplace-transform solution of Eq. (20) is straightforward but tedious. The solution for the Mth segment has the form

$$\theta_1(z,M) = \sum_{m=0}^{M}\alpha_m(M)\frac{\sin[\Omega(m\Delta s)z]}{\Omega(m\Delta s)}, \tag{21}$$

where the coefficients $\alpha_m(M)$ become progressively more complicated with increasing m. Examination of these coefficients for small values of m and M, however, shows that the ratio $\alpha_m(M)/\alpha_0(M)$ for $m < M$ is independent of M and decreases rapidly with m. This observation suggests that when the initial values of θ_1 and $d\theta_1/dz$ are independent of s, the signal at large M will be dominated by the $\Omega(0)$ term. Also, in a case where the initial perturbation is zero over the first $M-1$ slices, we expect that the dominant contribution to θ_1 will come from the $\Omega(M)$ term.

A computer program has been used to evaluate the series coefficients in Eq. (21) for arbitrary M. As expected, we find for small Δs that the resulting $\theta_1(z,M)$ values are effectively identical to the results of a single-particle simulation using the linearized continuum equations, and when Δs is increased to approximately the bucket length, the θ_1 fluctuations for large M increase a few percent in amplitude and shorten very slightly in wavelength. This result corroborates the use of the continuum model in the earlier simulations and indicates that the use of a discrete model in future simulations is unlikely to improve the problem of fluctuating wave phase.

3.2 Solution by separation of variables

The equation for the perturbed particle phase Eq. (15) may also be approximately solved by separation of variables. If we write θ_1 as the product

$$\theta_1(z,s) = F(z)G(s), \tag{22}$$

then we may readily calculate independent equations for F and G:

$$\frac{d^2F}{dz^2} = -\Omega^2(0)F(z) \tag{23a}$$

$$\left[\Omega^2(s) - \Omega^2(0)\right] G(s) = -\frac{K^2\eta_0}{\gamma_r}\int_0^s ds' G(s')\ \sin[\beta(s-s')]. \tag{23b}$$

The problem with this representation is that the initial conditions can not in general be satisfied by the separated solution. For the s-independent initial conditions of Eq. (18), the separated form of θ_1 is only valid when $G(s) \approx 1$. However, when we write G formally as $1+\epsilon(s)$, it is readily shown that

$$\epsilon(s) \approx \frac{\eta_0}{\gamma_r|\beta||\hat{a}(0)|}, \tag{24}$$

plus s-dependent terms of higher order. Since the beam-generated contribution to the equilibrium field is seen from Eq. (12) to be $\eta_0/(\beta\gamma_r)$ times a factor of the order of unity, the separation of θ_1 is approximately valid when

$$|\hat{a}_0(L_b)| \gg |\hat{a}(0)|. \tag{25}$$

Under this condition, which must be satisfied in any practical SWFEL, the perturbed particle phase is given approximately by

$$\theta_1(z,s) \approx \left(\frac{1+\frac{1}{2}a_w^2}{D_x a_w|\hat{a}(0)|}\right)^{1/2}\frac{\Delta\gamma_0}{\gamma_r}\ \sin[\Omega(0)z]. \tag{26}$$

This expression, which agrees with Eq. (21) in the limit of small Δs, is remarkable for several reasons. First, the phase-ripple amplitude for a given value of $\Delta\gamma_0/\gamma_r$ is seen to be independent of the beam current, the initial particle phase $\theta_0(s)$, and the signal frequency and wavenumber. Consequently, such wiggler parameters as the wavelength and cross-sectional dimensions as well as the FEL operating frequency and the beam energy and prebunching may be optimized without regard for FEL phase-stability. A second notable feature of Eq. (26) is that the input power P_{in} to the standing-wave cavities has a very weak effect on the phase-ripple amplitude, since $\theta_1 \sim P_{in}^{-1/4}$. The reason for this insensitivity is that, as the input power increases, the rate of phase change $\partial\phi/\partial s$ decreases like $P_{in}^{-1/2}$, but the length of beam where $|\hat{a}_0(s)| \approx |\hat{a}(0)|$ is correspondingly longer. Finally, the θ_1 estimate shows that phase ripple for a given $|\hat{a}(0)|$ is minimized by taking $a_w \approx 2^{1/2}$.

When the θ_1 approximation from Eq. (26) is used in Eq. (19) to calculate $\hat{a}_1$, we find that the resulting perturbation in wave phase ϕ_1 is given simply by

$$\phi_1 \approx -\theta_1 \tag{27}$$

Table 1 Simulation parameters for the standing-wave FEL

		nominal	optimized
average beam current	I_b	2.17 kA	4.45 kA
beam length	L_b	180.0 cm	
resonant energy	γ_r	27.6	16.7
wiggler strength	a_w	8.86	1.4
wiggler wavelength	λ_w	25 cm	37 cm
wiggler length	L_w	40 m	
waveguide height	h	3 cm	
waveguide width	w	10 cm	
signal frequency	$\omega_s/2\pi$	17.1 GHz	
cavity Q	Q	10^4	
input power	P_{in}	5 kW/m	
output energy	W_{out}	10 J/m	

in the region of the beam where $|\hat{a}_0(s)| \gg |\hat{a}(0)|$. This finding agrees with the observation in numerical simulations that the bucket phase $\theta + \phi$ is nearly constant and unaffected by nonzero $\Delta\gamma_0/\gamma_r$. We may also use $\hat{a}_1$ to estimate the final energy per unit length W_{out} expected from the SWFEL. Taking the initial wave phase to be zero, we obtain

$$W_{out}(z) \approx \frac{hw}{8\pi}\left(\frac{\omega_s}{c}\frac{m_e c^2}{e}\right)^2 |\hat{a}_0(L_b)|^2 \left[1 + \frac{2|\hat{a}(0)|\hat{a}_{0i}(L_b)}{|\hat{a}_0(L_b)|^2}\,\theta_1(z,L_b) - \frac{|\hat{a}(0)|\hat{a}_{0r}(L_b)}{|\hat{a}_0(L_b)|^2}\,\theta_1^2(z,L_b)\right]. \tag{28}$$

This expression indicates that ripple associated with the phase fluctuation is proportional to $|\hat{a}(0)|/|\hat{a}_0(L_b)|$ and therefore is normally quite small. An expression for $\Delta\gamma$ is trivially obtained from Eq. (8) by noting that $d\theta/dz = d\theta_1/dz$ and substituting Eq. (26) for θ_1:

$$\Delta\gamma \approx \Delta\gamma_0 \cos[\Omega(0)z]. \tag{29}$$

The energy is seen to oscillate about γ_r at the synchrotron frequency in the initial signal field with an amplitude given by the initial perturbation $\Delta\gamma_0$. Like the θ_1 variation, this oscillation is effectively independent of s.

4. NUMERICAL RESULTS

The analytic results of the previous section are verified and extended using the SWFEL simulation code described in Ref. 3. Linearized single-particle simulations are used here to directly check the phase-ripple scaling expected from Eq. (26), and further cases are run to show the effects of high input power. Also, multi-particle simulations, using the nonlinear SWFEL equations of Eqs. (3) - (6), are used to illustrate the effects of an s-dependent beam current and of realistic spreads in initial γ and θ values.

4.1 Initialization

Two sets of simulation parameters are listed in Table 1. The "nominal" values are those used in the previous SWFEL simulations[3], with no attempt made to optimize the wiggler strength and wavelength. The second set, labeled as "optimized" values, uses the a_w value expected to give the minimum phase ripple, and the wiggler wavelength has been adjusted to give a lower resonant energy. The average beam current has been selected in both cases to give an output energy per unit length of 10 J/m, which is an appropriate value for typical TBA designs.

Single-particle simulations are initialized by setting the initial θ for the particle to $\theta_0(s) = \alpha + \beta s$ and choosing the initial γ to be $\gamma_r + \Delta\gamma_0$. Analytic calculations show that a particle is not trapped if the initial bucket phase $\alpha+\phi(0)$ is greater than $\pi/2$ in magnitude, so in the simulations presented here, both α and $\phi(0)$ are taken to be zero. As in the previous simulations[3], the frequency-detuning parameter β is chosen to be π/L_b, and the reacceleration field is calculated from Eq. (13).

For multi-particle simulations, the initialization closely parallels the single-particle procedure. A distribution with prescribed spreads $\delta\theta_0$ and $\delta\gamma_0$ in θ_j and γ_j is loaded so that $\langle\theta_j\rangle = \alpha + \beta s$ and $\langle\gamma_j\rangle = \gamma_r + \Delta\gamma_0$. Simulation

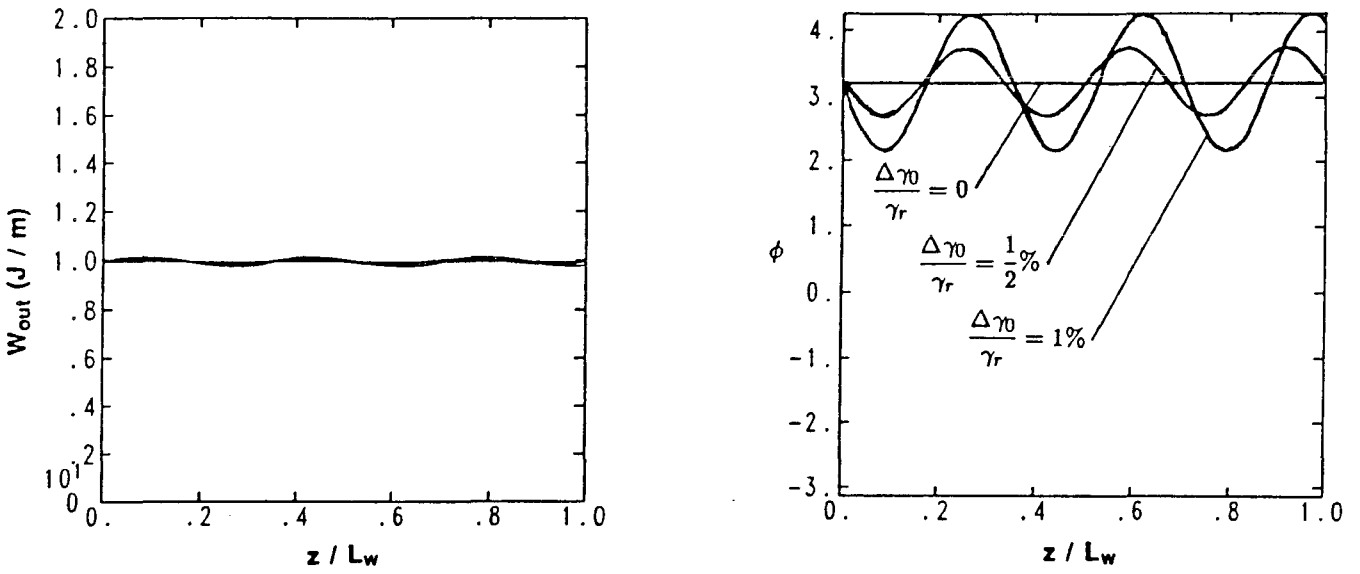

Fig. 1 Single-particle simulation of a standing-wave FEL for the nominal parameters using several values of $\Delta\gamma_0/\gamma_r$: (a) Output energy per unit length W_{out} and (b) wave phase ϕ as functions of z.

particles are uniformly distributed within this phase-space rectangle, and different random position are chosen for each beam slice. For the small spreads in θ_j and γ_j treated here, 200 simulation particles are adequate to give acceptably low statistical noise. The reacceleration field required to keep $\langle\gamma_j\rangle$ constant is given by

$$\frac{eE_z}{m_e c^2} = -D_x \frac{\omega_s}{c} a_w \left(\hat{a}_r \left\langle \frac{\sin\theta_j}{\gamma_j} \right\rangle + \hat{a}_i \left\langle \frac{\cos\theta_j}{\gamma_j} \right\rangle \right), \tag{30}$$

and as in the previous simulations[3], we calculate $E_z(s)$ at $z = 0$ and use it at all subsequent z positions.

In all simulations here, we set the initial signal level $|\hat{a}(0)|$ by assuming some input microwave power per unit length P_{in} and balancing this with cavity-wall losses, specified by an assumed cavity Q.

4.2 Single-particle simulations

The output microwave energy per unit length W_{out} and wave phase ϕ for a beam with the "nominal" parameters are shown in Fig. 1. As expected, the phase-ripple amplitude is seen to increase proportionally with $\Delta\gamma_0/\gamma_r$, and the magnitude is in good agreement with the analytic estimate of Eq. (26). A ripple amplitude of about 2% is expected in W_{out} from Eq. (28) for the case with $\Delta\gamma_0/\gamma_r = 1\%$, and we see roughly this fluctuation in Fig. 1. An examination of the wave and particle phases for successive values of s confirms that θ_1 is virtually independent of s and that the fluctuating part of ϕ is equal to $-\theta_1$ except for $s/L_b < 0.05$, as expected from Eq. (27). Also, the fluctuation of γ is found shifted in phase from θ_1 by $\pi/2$ and likewise independent of s, in agreement with Eq. (29).

The "optimized" parameters use a wiggler strength that is a factor of 6.3 smaller than the nominal value. According to Eq. (26), the phase ripple should then be reduced for these cases by a factor of about 0.55 from the nominal values. The phase plot the optimized parameters in Fig. 2 verifies this prediction, and a corresponding reduction in the W_{out} ripple is seen. The longer ripple wavelength seen in Fig. 2 results from the reduced synchrotron wavenumber Ω, which is proportional to $a_w^{1/2}$. Other simulation runs with a range of a_w values verify that $a_w = 2^{1/2}$ gives the minimum phase ripple for a given $|\hat{a}(0)|$ and that this ripple is insensitive to changes in other beam parameters.

The effects of increasing the input power P_{in} for the optimized parameters is shown in Fig. 3. The analytic estimate of θ_1, and hence ϕ_1, in Eq. (26) predicts that increasing P_{in} by a factor of sixteen should halve the phase-ripple amplitude. By comparison, the reduction seen when the input power increased from 5 kW/m to 80 kW/m is about 40%, and a further reduction of 35% occurs for an increase to 1280 kW. The analytic estimate

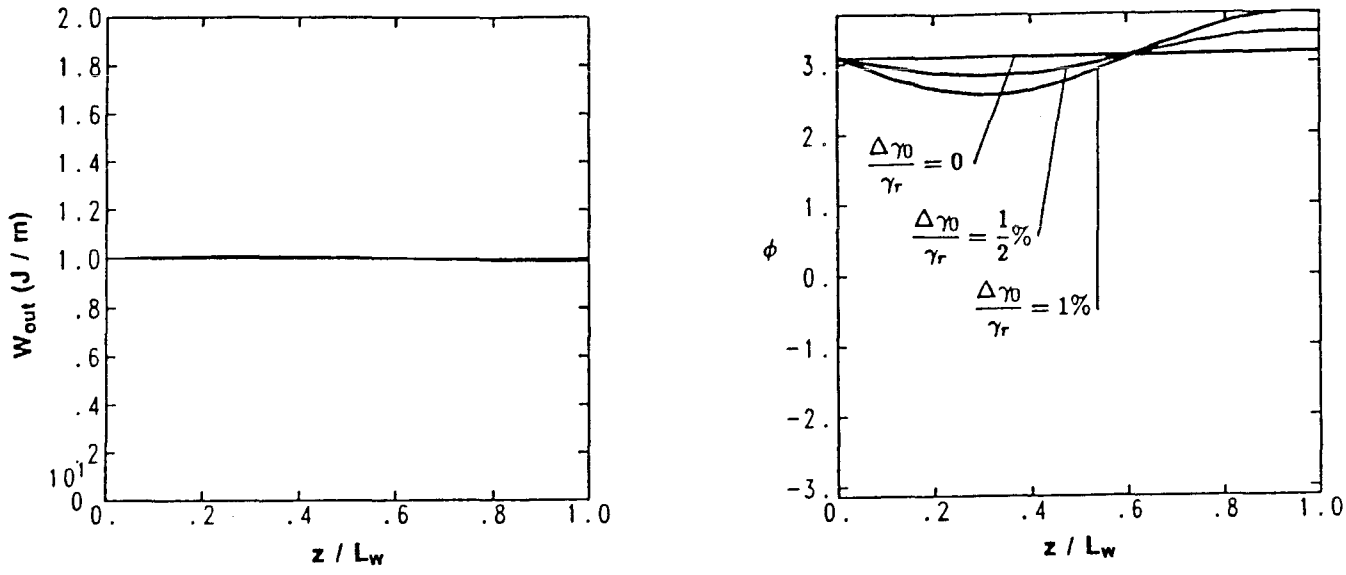

Fig. 2 Single-particle simulation of a standing-wave FEL for a set of "optimized" parameters with $a_w = 2^{1/2}$: (a) W_{out} and (b) ϕ as functions of z.

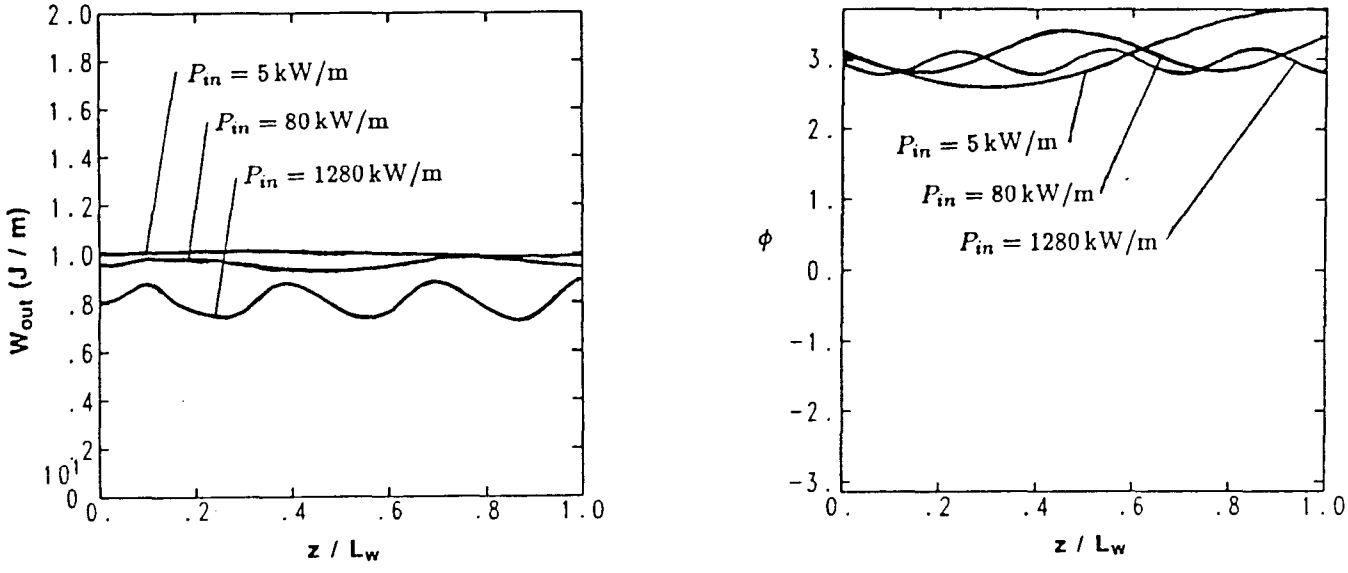

Fig. 3 Single-particle simulation of a standing-wave FEL for the "optimized" parameters using several values of input power P_{in}: (a) W_{out} and (b) ϕ as functions of z.

begins to fail for these high input-power values because the validity criterion of Eq. (25) is only marginally satisfied, with $|\hat{a}(0)|$ being about 10% of $|\hat{a}_0(L_b)|$. A second effect of high input power is seen in the W_{out} plot of Fig. 3. In addition to the expected sixteen-fold increase in the W_{out} ripple seen here, the average value of W_{out} decreases by about 20% as P_{in} is increased. The cause of this reduced cavity energy is the smaller reacceleration field found from Eq. (10) when $|\hat{a}(0)|$ is not negligible compared with $\eta_0/(|\beta|\gamma_r)$. Finally, examination of the γ for the case with high P_{in} shows that the variation in z is no longer sinusoidal, as expected from Eq. (29), but has a superimposed irregular component. This anharmonic motion, which results from the ripple in the $\hat{a}$ seen by the simulation particle over a synchrotron orbit, is benign for the single-particle distribution, but it leads to particle loss in multi-particle simulations.

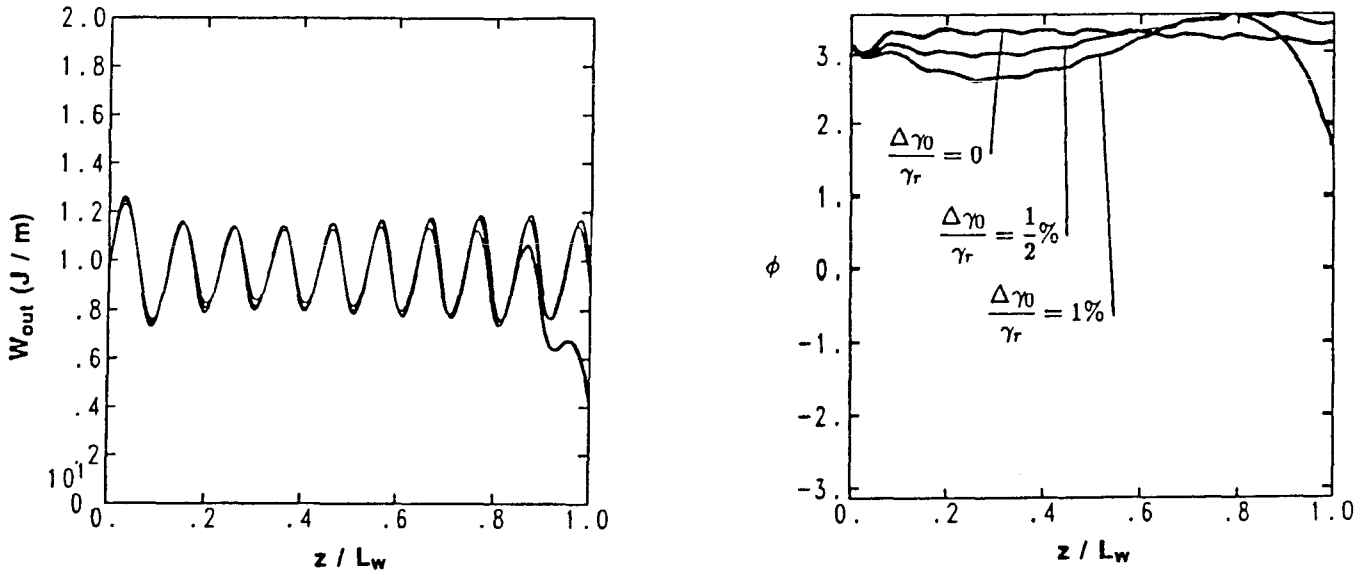

Fig. 4 Multi-particle simulation of a standing-wave FEL for the "optimized" parameters using a uniform distribution with $\delta\theta_0/2\pi = 0.1$ and $\delta\gamma_0/\gamma_r = 0.01$: (a) W_{out} and (b) ϕ as functions of z.

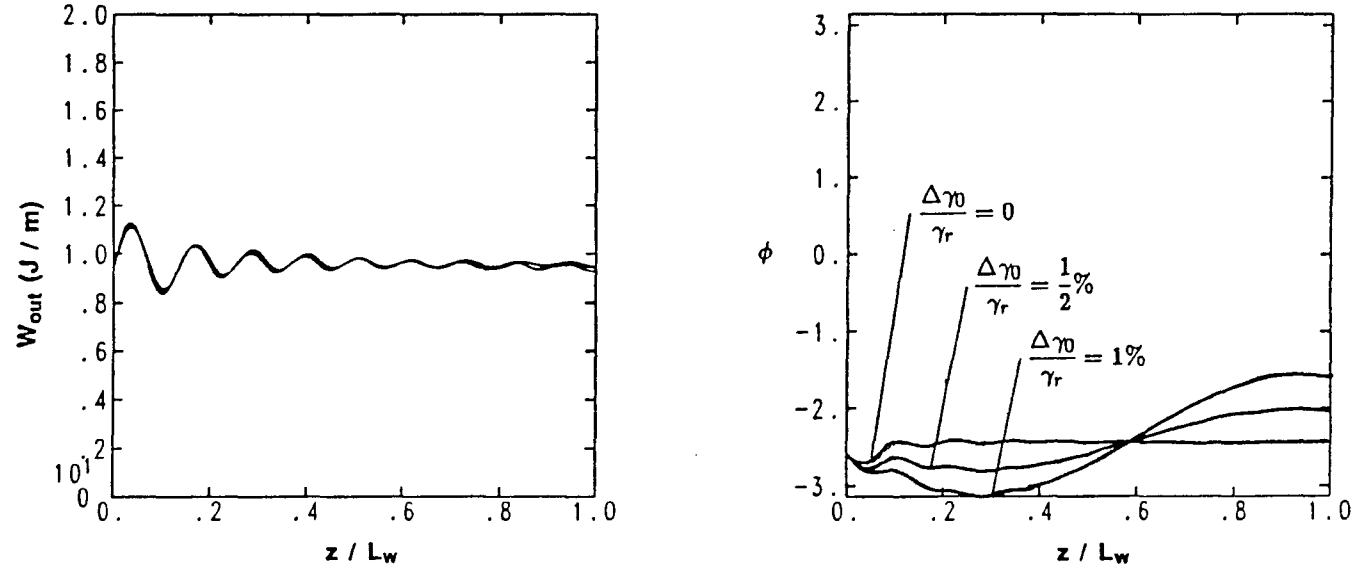

Fig. 5 Multi-particle simulation of a standing-wave FEL for the "optimized" parameters with a linearly increasing beam current: (a) W_{out} and (b) ϕ as functions of z.

4.3 Multi-particle simulations

The multi-particle simulations are useful for seeing the effects beam distributions with spreads in γ and θ and for determining the consequences of the signal-field terms in Eq. (3a), which were discarded in the linearized equations of Eq. (8). Both effects can be seen in the constant-current case shown in Fig. 4. Although the long-wavelength phase ripple here is similar to the single-particle results in Fig. 2, there is a superimposed ripple at the synchrotron frequency associated with $|\hat{a}(L_b)|$, due to the new terms in the θ_j equation. This high-frequency oscillation is strikingly evident in the W_{out} plot, where a 35% ripple is seen for all values of $\Delta\gamma_0/\gamma_r$. The ripple in signal amplitude is associated with a growing ripple in γ, and in the case with $\Delta\gamma_0/\gamma_r = 1\%$, it leads to detrapping of particles and an obvious drop in W_{out} and ϕ for $z/L_w > 0.8$.

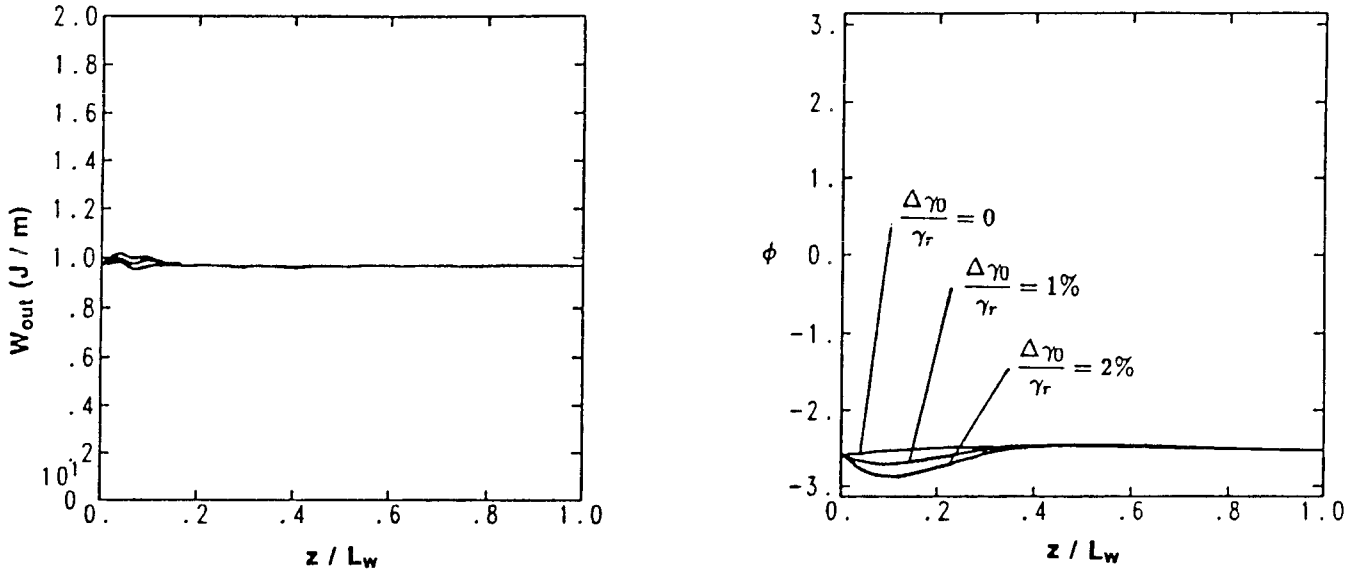

Fig. 6 Multi-particle simulation of a standing-wave FEL for the "optimized" parameters with a linearly increasing beam current and a $\Delta\gamma_0/\gamma_r$ that is zero at the head and increases to the indicated value near $s/L_b = 0.2$.: (a) W_{out} and (b) ϕ as functions of z.

The phase-space acceptance in a SWFEL was found in earlier work to be improved by having the current increase linearly with s. Figure 5 shows the results of a multi-particle simulation using the optimized parameters, but having a linear current ramp instead of having constant current. In this case, the peak current must be about twice the average value in Table 1 in order to give the same W_{out}. The phase ripple is seen to be about 20% higher than the constant-current case in Fig. 4, but the high-frequency ripple in W_{out} damps with increasing z, and no particles are lost.

Finally, we note that for either constant or ramped current, most of the phase ripple is introduced in the part of the beam head where $|\hat{a}_0(s)| \approx |\hat{a}(0)|$. A clear demonstration of this assertion is shown in Fig. 6. In this case, the initial average beam energy is taken to have the s-dependent form

$$< \gamma_j >= \gamma_r \left[1 + \frac{\Delta\gamma_0}{\gamma_r} \frac{1}{1 + \exp\left(\frac{s - s_0}{\delta s}\right)} \right], \tag{31}$$

where we set $s_0/L_b = 0.2$ and $\delta s/L_b = 0.05$. The ϕ plot for this case shows a transient phase fluctuation of less than a half radian and no significant phase fluctuation for $z/L_w > 0.4$. Similarly, W_{out} shows some small initial variation but is effectively constant for $z/L_w > 0.2$. This finding indicates that the beam energy needs to be near γ_r for at most only the first 20% of the beam for the signal phase and amplitude to remain nearly constant.

5. CONCLUSIONS

The approximate analytic solution for the response of a standing-wave FEL to small errors of the drive-beam energy, given by Eqs. (26) - (29), indicates that such errors lead to a ripple in the final wave phase with a wavelength in z equal to the synchrotron wavelength in the initial signal field. This phase ripple develops near the beam head during the time when the signal amplitude $|\hat{a}(s)|$ is near the initial value $|\hat{a}(0)|$, and it is in effect "frozen in" when the signal becomes larger because $\partial\phi/\partial s \sim |\hat{a}|^{-1}$. The ripple amplitude is proportional to the initial fractional error in the beam energy $\Delta\gamma_0/\gamma_r$ and is minimized by choosing the dimensionless wiggler strength a_w to be about $2^{1/2}$. For practical initial levels of the signal field $|\hat{a}(0)|$ in the range of 0.001 to 0.01, this optimal a_w value still leads to a phase-ripple amplitude of roughly $18 - 56\ \Delta\gamma_0/\gamma_r$. Larger values of $|\hat{a}(0)|$ lead to increasing ripple in the output signal energy per unit length W_{out}, while smaller values reduce the phase-space acceptance of the device. Numerical simulations using single-particle and multi-particle distributions corroborate the analytic results and

indicate further that the phase ripple is not improved by changes in the axial dependence of the beam current, although taking the current to increase monotonically from zero at the head improves the acceptance.

The acceptable level of phase fluctuations along the wiggler may be estimated from the requirements of a two-beam accelerator. The allowable relative momentum spread $\Delta P/P$ for linear colliders is determined by the chromatic acceptance of the final focus, and the value in typical recent designs is about 0.1%. Since the momentum P of the high-energy beam in a coupled-cavity TBA is given crudely by

$$P \sim \int_0^{L_w} dz\ W_{out}^{1/2} \cos\phi_1, \tag{32}$$

the analytic results of Eqs. (26) - (28) give

$$\frac{\Delta P}{P} \approx \frac{1}{4}\left(\frac{1+\frac{1}{2}a_w^2}{D_x a_w |\hat{a}(0)|}\right)\left(\frac{\Delta\gamma_0}{\gamma_r}\right)^2. \tag{33}$$

This momentum error comes entirely from the wave-phase ripple ϕ_1 because the dominant error arising from W_{out} is smaller by a factor of the order of $|\hat{a}(0)|/|\hat{a}(L_b)|$. If we take $a_w = 2^{1/2}$ and $|\hat{a}(0)| = 0.001$, than Eq. (33) indicates that the maximum allowable beam-energy error is $\Delta\gamma_0/\gamma_r \approx 0.1\%$, corresponding to a phase ripple with an amplitude of 0.06 radian. Although this degree of energy reproducibility has not been achieved in existing induction linear accelerators, the numerical simulations here indicate that the beam-energy requirement need only be satisfied over the initial section of the pulse. If the beam current is taken to increase linearly from zero over the length of the pulse, than the current remains relatively low near the beam head. With such a pulse format, the reduced beam loading near the head should simplify the design of repeatable pulsed-power units.

6. ACKNOWLEDGMENTS

Work performed under the auspices of the U. S. Department of Energy by Lawrence Livermore National Laboratory under contract W-7405-ENG-48 and by Lawrence Berkeley Laboratory under contract DE-AC03-76SFF00098 and by the U. S. Department of Energy Division of High-Energy Physics

7. REFERENCES

1. A. M. Sessler, in *Laser Acceleration of Particles*, AIP Conf. Proc. 91, edited by P. J. Channell (AIP, New York, 1982), p. 154.
2. D. B. Hopkins, private communication
3. W. M. Sharp, A. M. Sessler, D. H. Whittum, and J. S. Wurtele, "Simulation of a Standing-Wave Free-Electron Laser", proceeding of the 1990 Linear Accelerator Conference (10-14 September 1990, Albuquerque, NM) (to be published.
4. A. M. Sessler, D. H. Whittum, W. M. Sharp, M. A. Makowski, and J. S. Wurtele, "The Coupled-Cavity Free-Electron Laser Two-Beam Accelerator", to be published.
5. H. Henke, CLIC Note 59, March 1988.
6. A. W. Chao, B. Richter, and C. Y. Yao, *Nucl. Instrum. Methods* **178**, 1 (1980).